J Mater Sci (2009) 44:1594–1599
DOI 10.1007/s10853-008-3229-2

Annealing effect on the structural, optical, and electrical properties of $CuAlO_2$ films deposited by magnetron sputtering

W. Lan · W. L. Cao · M. Zhang · X. Q. Liu · Y. Y. Wang · E. Q. Xie · H. Yan

Received: 4 September 2008 / Accepted: 23 December 2008 / Published online: 27 January 2009
© Springer Science+Business Media, LLC 2009

Abstract We studied the annealing effect on the structural, optical, and electrical properties of sputtered $CuAlO_2$ films. It is found that the crystallinity of $CuAlO_2$ films is improved with increasing the annealing temperature in N_2 ambient, and the film annealed at 900 °C presents the excellent preferred (001) orientation in X-ray diffraction patterns as well as Raman scattering signals, A_{1g} and E_g. The optical absorption edge of the annealed films is observed extremely complex. Four optical bandgaps estimated are distributed in the following energy regions: ~3.00, ~3.15, ~3.50, and ~3.75 eV, which might originate from different direct transitions in $CuAlO_2$ energy band, respectively. For the annealed $CuAlO_2$ films, the resistivity decreases three orders of magnitude, which is attributed to the contribution of intrinsic defects, Cu vacancy and interstitial oxygen.

Introduction

Transparent conductive oxides (TCOs) are widely applied as transparent electrodes in flat panel displays, solar cells, and touch panels. The main reason for the lack of TCO-based devices is the absence of high-conductivity *p*-type TCOs. However, the delafossite-structure $CuAlO_2$ film was first achieved in 1997 as a candidate to be a highly conductive p-type TCO [1]. The discovery has stimulated interest in developing transparent oxide optoelectronic devices such as laser diodes, light-emitting diodes, and transistors using an appropriate combination of *p*- and *n*-type TCO films. So far, $CuAlO_2$ films have been synthesized by various deposition techniques, such as pulsed laser deposition [1, 2], plasma-enhanced chemical vapor deposition [3], sputtering [4–6], sol–gel [7], spray pyrolysis [8], and so on. In comparison, the main advantage of sputtering method is compatible with microelectronics applications in large-area deposition techniques, which is beneficial to the wider application of $CuAlO_2$ film. However, as-sputtered $CuAlO_2$ films exhibit the inferior structure, which results in the low *p*-type conductivity and optical transmittance [4, 5, 9]. It is well known that the annealing is a very effective technique to improve the structural properties of materials. Therefore, the annealing technique is employed for as-sputtered $CuAlO_2$ film to look forward to developing its electrical and optical properties. Up to now, there are few reports on the systematic investigation of the annealing for $CuAlO_2$ films.

In this study, $CuAlO_2$ films were deposited by radio frequency (RF) magnetron sputtering on quartz substrates. Then, these films were conducted the annealing treatment at different temperatures in N_2 ambient. We mainly focus on the influence of the annealing on the structural, electrical and optical properties of $CuAlO_2$ films. In addition, it is worth pointing out that Raman scattering is applied to analyze the structure of $CuAlO_2$ films.

W. Lan (✉) · W. L. Cao · X. Q. Liu · Y. Y. Wang · E. Q. Xie
Department of Physics, School of Physical Science and Technology, Lanzhou University, Lanzhou 730000, People's Republic of China
e-mail: lanw@lzu.edu.cn

W. Lan · M. Zhang · H. Yan
The College of Materials Science and Engineering, Beijing University of Technology, Beijing 100022, People's Republic of China

Experimental details

$CuAlO_2$ films were deposited on quartz substrates using RF magnetron sputtering. The sputtering target was prepared

Table 1 Deposition conditions for fabricating $CuAlO_2$ film by RF magnetron sputtering

Parameter	Value
Sputtering power	100 W
Work pressure	1 Pa
Substrate temperature	500 °C
Electrode distance	40 mm
Sputtering gasses	Ar and O_2 (4:1 flow ratio)
Deposition time	2 h

by solid-state reactions of $Al(OH)_3$ and Cu_2O [9]. Quartz substrates were cleaned ultrasonically using methylbenzene, acetone and ethanol in turn. The chamber was pumped up to 6×10^{-3} Pa using a turbomolecular pump and the target was pre-sputtered for 10 min to remove contamination on the surface. The summary of deposition conditions is shown in Table 1. The annealing process was performed in a tubular furnace with a sealing Al_2O_3 pipe and a Pt–Rh thermocouple. A warming temperature speed is 5 °C/min and a natural cooling was maintained after finishing the annealing.

The structure of $CuAlO_2$ films was charactered by Bruker-AXS D8 X-ray diffractometer (Cu kα, $\lambda = 0.15406$ nm) and Raman scattering spectrometer with a confocal microscope (Horiba Jobin-Yvon Labram HR800). In X-ray diffraction (XRD) operation, the $2\theta/\theta$-coupled scan mode was used with scan step of 0.02°, and scan time of 0.3 s/step, and the scan procedure was performed continually two times. Raman spectra were excited using the 532-nm line of a YAG doubled diode laser, and analyzed by the last grating of the spectrometer with a spectral resolution better than 1 cm^{-1}. The thickness of $CuAlO_2$ films was controlled to be around 200 nm, which was detected by a Seimitzu Surfcom 480A profiler. UV–Vis spectrophotometer (SHIMADZU, UV-3101) was used to determine the optical properties of $CuAlO_2$ films. Electrical conductivity was measured by means of the automatic measurement system assembled by Agilent E5273 and Lakeshore 340. The conductivity type was detected by Hall effect with the four-probe method in Van der Pauw configuration.

Results and discussion

Structural properties

An as-deposited $CuAlO_2$ film on quartz substrate was sectioned into several small samples with 0.7×0.7 cm^2. One sample was annealed in air for 3 h at 900 °C, whereas the others were annealed in N_2 ambient for 5 h at different temperatures: 700, 800, 900, and 1,000°C. Figure 1 shows XRD patterns of $CuAlO_2$ films as-deposited and annealed.

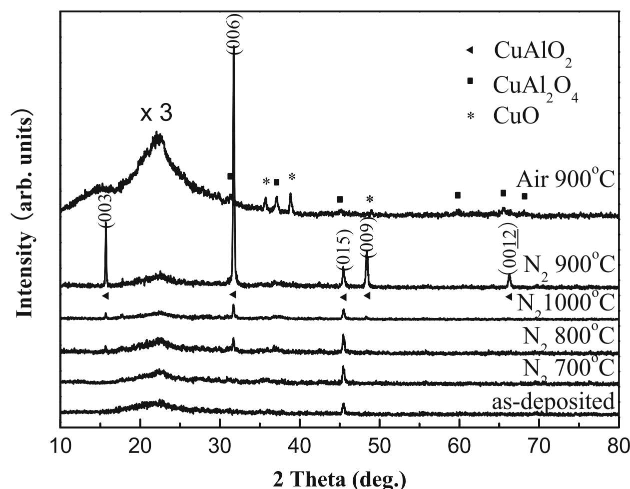

Fig. 1 XRD patterns of $CuAlO_2$ films as-deposited and annealed in N_2 ambience at different temperatures

The as-deposited $CuAlO_2$ film just appears at (015) diffraction peak of delafossite-structure $CuAlO_2$ (PDF 76-2398) [10]. After being annealed in air, several new peaks emerge in the XRD pattern instead of the (015) peak. These peaks originate from the reflections of $CuAl_2O_4$ (PDF: 33-0448) [11] and CuO (PDF: 74-1021) [12], which supports the fact that $CuAlO_2$ phase is decomposed into a mixture of $CuAl_2O_4$ and CuO in air via the following reaction:

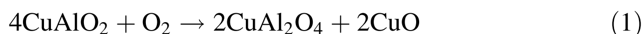

$$4CuAlO_2 + O_2 \rightarrow 2CuAl_2O_4 + 2CuO \quad (1)$$

This also suggests that a protective atmosphere, such as N_2, should be used to avoid the decomposition of $CuAlO_2$ films during the high-temperature annealing. As seen from Fig. 1, the decomposition behavior does not take place when $CuAlO_2$ films are annealed in N_2 ambient conditions. When the annealing temperature of the film reaches 800 °C, (003) and (006) diffraction peaks associated with $CuAlO_2$ begin to appear, indicating that the atoms rearrange in the (001) crystal plane parallel to the substrate surface. The rearrangement is of advantage to the electrical conduction for *p*-type $CuAlO_2$ film. At the annealing temperature of 900 °C, the other two diffraction peaks (009) and (0012) also come into view and the intensity of these peaks becomes much stronger, which imply that the surface energy of the (001) crystal plane might be the lowest in $CuAlO_2$ lattice. As the annealing temperature is further enhanced, the weakened crystallinity is correlated with the appearance of microscopic cavities in $CuAlO_2$ film observed by atomic force microscope (not shown).

As reported by Pellicer-Porres et al. [13], the delafossite-structure $CuAlO_2$ belongs to $R\overline{3}m$ spatial group, and the primitive unit cell contains four atoms, giving raise to 12 normal modes. The vibrations at the Γ point can be decomposed as $\Gamma = A_{1g} + E_g + 3A_{2u} + 3E_u$. Among these, the $A_{1g} + E_g$ are Raman active modes. So we could apply

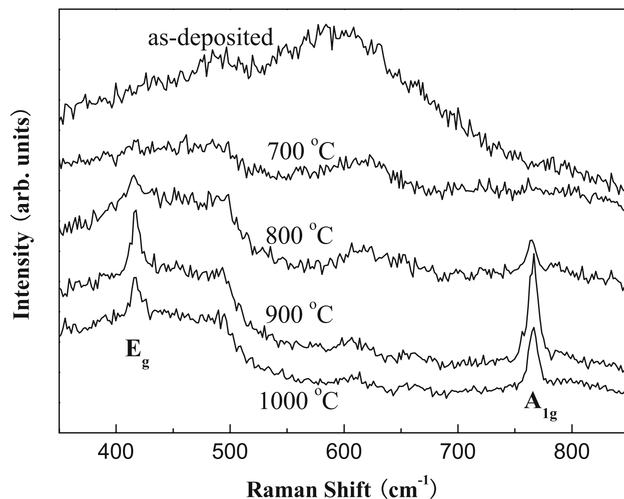

Fig. 2 Raman scattering spectra of $CuAlO_2$ films as-deposited and annealed in N_2 ambience at different temperatures

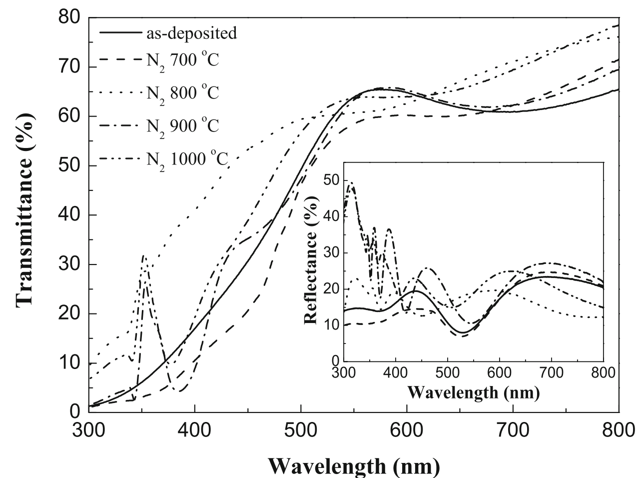

Fig. 3 Optical transmittance and reflectance spectra of $CuAlO_2$ films as-deposited and annealed in N_2 ambience at different temperatures

Raman scattering to further identify the structural properties of $CuAlO_2$ films. Figure 2 shows Raman scattering spectra of $CuAlO_2$ films as-deposited and annealed at different temperatures in N_2 ambience. Two Raman shift peaks are found around 767 and 420 cm^{-1} for all the annealed films, and they could be attributed to A_{1g} and E_g Raman modes of $CuAlO_2$ [13], respectively. A hump near 600 cm^{-1} might be due to quartz substrate. Raman signals become intense gradually with the increase of the annealing temperature, and the excellent A_{1g} and E_g Raman peaks are obtained at 900 °C. The intensity change of the Raman peaks is in accordance with the above depicted XRD results. In addition, we observe that the A_{1g} Raman peaks are always stronger than the E_g for the annealed $CuAlO_2$ films. Based on the theoretical and experimental investigation of Raman scattering for the delafossite $CuAlO_2$ crystal, the A_{1g} Raman mode reveals the vibration in the orientation of the Cu–O bonds parallel to the *c* axis, whereas the E_g describes movement in the perpendicular direction. Therefore, the stronger A_{1g} Raman peak also indicates that the annealed $CuAlO_2$ films grow along the preferred orientation of (001) perpendicular to the substrate surface.

Optical properties

Figure 3 shows optical transmittance and reflectance spectra of $CuAlO_2$ films as-deposited and annealed in N_2 ambience. As seen, at the wavelength region of 500–800 nm, no significant change takes place on the optical transmittance spectra, and the transmittance is around 50–80% for all $CuAlO_2$ films. However, it is worth noting that an obvious change occurs on the transmittance spectra below the wavelength of 500 nm, especially around 353 nm. Compared with the others, the film annealed at 800 °C exhibits a high transmittance in the range of 300–500 nm, and a weak transmittance peak begins to emerge at 353 nm. With the increment of the annealing temperature, the transmittance peak gradually becomes prominent. It is well known that the incident photons in this region have sufficient energy to excite electrons from the valence band to the conduction band. Thus this region carries the information of the bandgap of the material. According to the transmittance, the reflectance (inset in Fig. 3), and the film thickness, we can estimate direct optical bandgap (E_g) of $CuAlO_2$ film by means of the equation: $(\alpha h\nu)^2 = A(h\nu - E_g)$. This method was depicted in our previous report [9] in detail. The fitting results are exhibited in Fig. 4 for all the $CuAlO_2$ films. Except for the as-deposited with one E_g value, all the annealed films could be deduced to three E_g values from the $(\alpha h\nu)^2$*vs.* $h\nu$ plots. These E_g values are summarized in Table 2 and classified into four different energy-regions: ~3.00, ~3.15, ~3.50, and ~3.75 eV. Moreover, the E_g values of the films annealed at 800–1,000 °C are very close, suggesting that they have similar band structure.

A lot of study has been done on the band-structure calculation of $CuAlO_2$ in the last few years [2, 14–16]. It is found that $CuAlO_2$ is an indirect bandgap semiconductor and its band edges are very complex, especially the valence-band maximum (VBM). The conduction-band minimum is generally believed to situate at Γ point in Brillouin zone. However, there are very serious divergences in the VBM position and bandgap value. Yanagi et al. [2] and Ingram et al. [14] found that the VBM located at *F* point in Brillouin zone employing the full-potential linearized augmented plane wave (FLAPW) to calculate the energy band of $CuAlO_2$. The indirect bandgap *F*-Γ was calculated to be 1.7–1.95 eV, and the direct bandgap Γ–Γ was 2.7–2.8 eV. Using the first-principles method, Nie

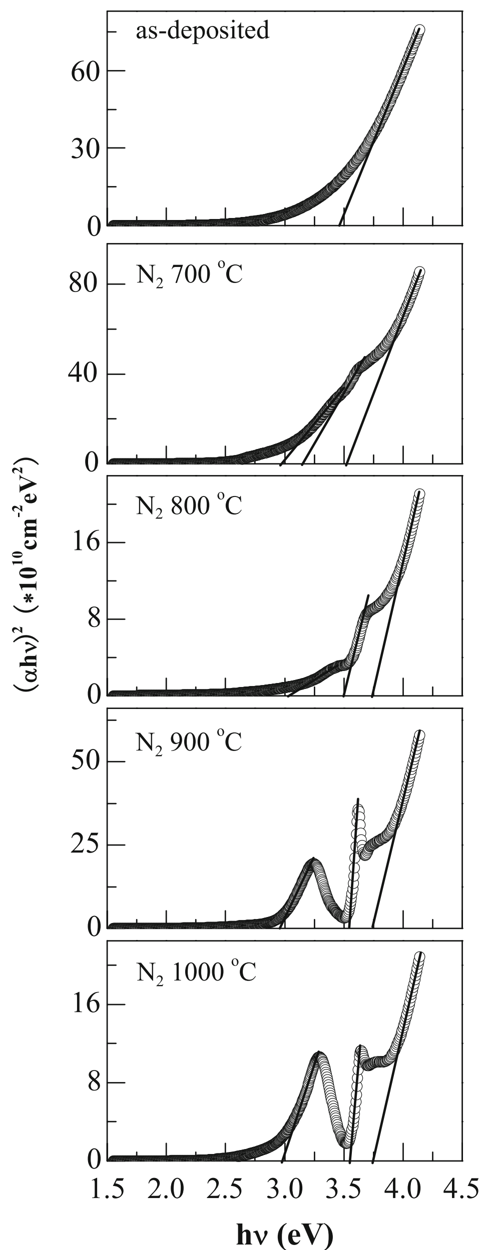

Fig. 4 Fitting process of direct bandgaps of $CuAlO_2$ films as-deposited and annealed in N_2 ambience at different temperatures

Table 2 Summary of direct bandgaps for $CuAlO_2$ films as-deposited and annealed in N_2 ambience at different temperatures

	Bandgap			
	I (eV)	II (eV)	III (eV)	IV (eV)
As-deposited	–	–	3.46	–
700 °C	2.97	3.15	3.52	–
800 °C	3.04	–	3.50	3.74
900 °C	2.96	–	3.55	3.75
1,000 °C	2.97	–	3.55	3.75

et al. [15] observed that the VBM occured on the Γ–*F* line near *F* point. The indirect and direct bandgaps were determined to be 1.97 and 2.93 eV, respectively. They also believed the lowest direct band-to-band transition took place between *L* and *L* points with the energy 2.68 eV. On the basis of the ab initio electronic structure calculation and the experimental results for $CuAlO_2$ single-crystal and films, Pellicer-Porres et al. [17] recently observed that the VBM located at *X* point in Brillouin zone and several electron transitions might exist. In their calculations, the indirect transition with the energy 2.99 eV would occur between Γ–*X* points and the direct transition with the lowest energy took place at the *P*–*P* points. Hence, there is no accredited standpoint on the electronic structure of $CuAlO_2$ in the theoretical research aspect. On the other hand, the reported experimental results were also at variance on the optical bandgap of $CuAlO_2$. Benko and Koffyberg [18] found that the indirect bandgap was 1.65 eV. Kawazoe et al. [1, 19] and Yanagi et al. [2] observed that the direct and indirect bandgaps were 3.5 eV and 1.8 eV, respectively. The direct bandgaps with 3.75 eV were evaluated by Banerjee et al. [6]. In other literatures [4, 8], they found that the direct bandgap was varying in energy from 3.34 to 3.94 eV. Cai et al. [20] observed two direct optical bandgaps in the plot of $(\alpha h\nu)^2$ *vs.* $h\nu$, in which the smaller was in the range of 2.9–3.6 eV, the larger in the range of 4.5–4.7 eV for the films with the dominant $CuAlO_2$ phase. Recently, Yu et al. [21] obtained the direct bandgap of 3.11–3.27 eV for *N*-doped $CuAlO_2$ films prepared by direct current reactive sputtering. All these cases indicate that the energy band of $CuAlO_2$ film is extremely complicated, and the optical bandgap depends heavily on the preparation method of $CuAlO_2$ film. Therefore, now we could not exactly determine whether these optical bandgaps estimated from the as-deposited/annealed $CuAlO_2$ films do relate with some direct band-to-band transition type or with the transition between band and intrinsic acceptor level, respectively. A more powerful research is needed in this aspect, which is our further aim for a future study.

Electrical properties

Through the annealing treatment in protective atmosphere, $CuAlO_2$ films show preferred *c* orientation, which is expected to improve the electrical properties. The current–voltage (I–V) characteristics of $CuAlO_2$ films as-deposited and annealed were accomplished at room temperature (in Fig. 5). Ag electrodes as-sputtered were subjected to in situ thermal treatment in vacuum at 400 °C. In the I–V plots, the linear dependence relationships under both forward and reverse electrical fields indicate that ohmic contacts have been formed between Ag electrodes and $CuAlO_2$ films. The

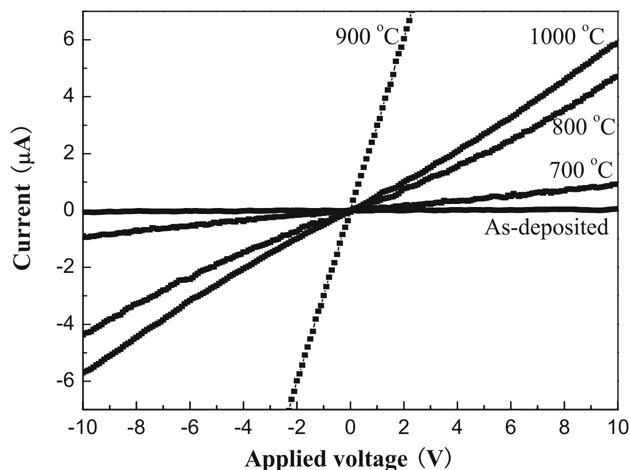

Fig. 5 I–V characteristics of $CuAlO_2$ films as-deposited and annealed in N_2 ambience at different temperatures

average resistivities were calculated to be 4.62×10^4, 2.28×10^3, 5.21×10^2, 3.70×10^1, and 3.78×10^2 Ω cm for the films as-deposited and annealed at 700, 800, 900, and 1,000 °C, respectively. The resistivity decreases three orders of magnitude after $CuAlO_2$ films are annealed, and the smallest resistivity is obtained at 900 °C. This result demonstrates that the annealing technique is advantageous for enhancing the electrical conduction of $CuAlO_2$ film. In addition, the Hall effect measurement for $CuAlO_2$ film with the smallest resistivity reveals Hall coefficient, mobility, and carrier concentration to be 183.6 $cm^3\ C^{-1}$, $3.40 \times 10^{16}\ cm^{-3}$, and 4.07 $cm^2\ V^{-1}\ s^{-1}$, respectively. The positive Hall coefficient confirms that $CuAlO_2$ film belongs to *p*-type semiconductor.

As far as wide bandgap semiconductors are concerned, defect chemistry plays a very important role in their electrical conduction. For instance, the intrinsic defects, oxygen vacancy, and interstitial zinc, are the primary origins of electrical conduction for *n*-type undoped ZnO films [22]. Intrinsic *p*-type TCO semiconductor should be similar with *n*-type TCO in the conduction mechanism. For *p*-type $CuAlO_2$ film, several intrinsic defects, such as Cu vacancy, Al vacancy, and interstitial oxygen, might contribute to its electrical conduction. First, Kawazoe et al. [1] supposed that positive hole carriers might be induced by excess oxygen in *p*-type $CuAlO_2$ film. By measuring oxygen concentration in $CuAlO_2$ films, Banerjee et al. [23] found that the conductivity was enhanced with increasing excess oxygen concentration, whereas when the excess oxygen exceeded a certain concentration, the conductivity of the films began to reduce. On the other hand, Katayama-Yoshida group [24, 25] performed ab initio total energy calculation on native point defects to explore the conduction mechanism of *p*-type $CuAlO_2$. The relevant defects, Cu vacancy, and interstitial oxygen, have relatively low formation energies. Interstitial oxygen and Al vacancy induce deep defect levels, while Cu vacancy induces no deep levels. Therefore, Cu vacancy and interstitial oxygen are easily formed during the growing process of $CuAlO_2$ film, and Cu vacancy is believed to be the primary contributor of the *p*-type conductivity. We assume that two acceptor defects (Cu vacancy and interstitial oxygen) just exist in $CuAlO_2$ film, and then the nonstoichiometric defect reaction can be represented by the following equation:

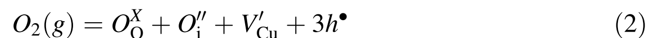

$$O_2(g) = O_O^X + O_i'' + V_{Cu}' + 3h^{\bullet} \qquad (2)$$

where O_O, O_i, V_{Cu}, and h denote lattice oxygen, interstitial oxygen, Cu vacancy, and hole, respectively. Superscripts X, $'$ and $\bullet$ denote effective neutral, negative, and positive charge states, respectively. This equation expresses the introduction of hole carriers ionized by Cu vacancy and interstitial oxygen in the excess oxygen condition. The more the Cu vacancy and interstitial oxygen in $CuAlO_2$ film, the more the hole carriers that get ionized, which is in favor of the enhancement of *p*-type conductivity. On the contrary, the abundant acceptor defects also play roles of scattering centers for hole carriers, which result in the decline of carrier mobility in the film. Altogether, we have to pursue the maximizing of the product of hole carrier concentration and carrier mobility to enhance the electrical conductivity of $CuAlO_2$ film as soon as possible.

Conclusions

$CuAlO_2$ films sputtered on quartz substrates were conducted the annealing at 700–1,000°C in N_2 ambience. The film annealed at 900°C shows the excellent preferred *c* orientation as well as two strong Raman scattering peaks located at 767 (A_{1g}) and 420 cm^{-1} (E_g), associating with the delafossite-structure $CuAlO_2$. Optical transmittance spectra exhibit that $CuAlO_2$ films are transparent (50–80%) in the visible range. The extremely complex absorption edges are observed for the annealed films. Using the linear fitting, four direct bandgaps are estimated to distribute in different energy regions: ~3.00, ~3.15, ~3.50, and ~3.75 eV, which might be related with the different direct transitions in $CuAlO_2$ energy bands. The resistivity of *p*-type $CuAlO_2$ films is reduced to three orders of magnitude via the annealing treatment. We believe that intrinsic defects, Cu vacancy, and interstitial oxygen, play important roles in the decrease of electrical resistivity.

Acknowledgements The authors would like to acknowledge the financial support by the National Natural Science Foundation of China (No. 50802037), the Excellent Persons in Science and Engineering of Beijing (20061D0501500199), and the Youth Teacher Sustentation Plan of School of Physical Science and Technology of Lanzhou University (No. WL200705).

References

1. Kawazoe H, Yasukawa M, Hyodo H, Kurita M, Yanagi H, Hosono H (1997) Nature 389:939
2. Yanagi H, Inoue S, Ueda K, Kawazoe H, Hosono H, Hamada N (2000) J Appl Phys 88:4159
3. Gong H, Wang Y, Luo Y (2000) Appl Phys Lett 76:3959
4. Banerjee AN, Chattopadhyay KK (2005) J Appl Phys 97:084308
5. Ong CH, Gong H (2003) Thin Solid Films 445:299
6. Banerjee AN, Kundoo S, Chattopadhyay KK (2003) Thin Solid Films 440:5
7. Tonooka K, Shimokawa K, Nishimura O (2002) Thin Solid Films 411:129
8. Bouzidi C, Bouzouita H, Timoumi A, Rezig B (2005) Mater Sci Eng B 118:259
9. Lan W, Zhang M, Dong GB, Dong PM, Wang YY, Yan H (2007) Mater Sci Eng B 139:155
10. Ishiguro T, Ishizawa N, Mizutani N, Kato M, Tanaka K, Marumo F (1983) Acta Crystallogr, B: Struct Sci 39:564. Calculated from ICSD using POWD-12 ++, (1997)
11. Lambert JC, Eysel W (1980) Mineralogical-Petrograph. Institute, Universitat Heidelberg, ICDD Grant-in-Aid, Germany
12. Tunell G, Posnjak E, Ksanda CJ, Kristallogr Z (1935) Kristallgeom Kristallphys Kristallchem 90:120. Calculated from ICSD using POWD-12 ++, (1997)
13. Pellicer-Porres J, Martínez-García D, Segura A, Rodríguez-Hernández P, Muñoz A, Chervin JC, Garro N, Kim D (2006) Phys Rev B 74:184301
14. Ingram BJ, Mason TO, Asahi R, Park KT, Freeman AJ (2001) Phys Rev B 64:155114
15. Nie X, Wei SH, Zhang SB (2002) Phys Rev Lett 88:066405
16. Jayalakshmi V, Murugan R, Palanivel B (2005) J Alloys Compd 388:19
17. Pellicer-Porres J, Segura A, Gilliland AS, Muñoz A, Rodríguez-Hernández P, Kim D, Lee MS, Kim TY (2006) Appl Phys Lett 88:181904
18. Benko FA, Koffyberg FP (1984) J Phys Chem Solids 45:57
19. Kawazoe H, Yanagi H, Ueda K, Hosono H (2000) Mater Res Bull 8:28
20. Cai JL, Gong H (2005) J Appl Phys 98:033707
21. Yu RS, Liang SC, Lu CJ, Tasi DC, Shieu FS (2007) Appl Phys Lett 90:191117
22. Zhang SB, Wei SH, Zunger A (2001) Phys Rev B 63:075205
23. Banerjee AN, Maity R, Ghosh PK, Chattopadhyay KK (2005) Thin Solid Films 474:261
24. Katayama-Yoshida H, Koyanagi T, Funashima H, Harima H, Yanase A (2003) Solid State Commun 126:135
25. Katayama-Yoshida H, Sato K, Kizaki H, Funashima H, Hamada I, Fukushima T, Dinh VA, Toyoda M (2007) Appl Phys A 89:19